

# Casimir expulsion of shifted configurations

Evgeny G. Fateev\*

*Institute of mechanics, Ural Branch of the RAS, Izhevsk 426067, Russia*

(Dated: October 9, 2018)

The shift of nanosized metal configurations relative to one another can lead to an increase in the range of optimal lengths of wings and angles of the opening of cavities, at which noncompensated Casimir forces in them are maximal. The possibility of the existence of the effect of Casimir expulsion is demonstrated with a trapezoid cavity with shifted wings which are opened at different angles. It is also shown that shift in parallel structures leads to the appearance of forces tending to bring the configuration back to the situation before the shift. In some conditions, in systems with shifted structures there are moments of torsion and complex oscillation processes.

PACS numbers: 03.70.+k, 04.20.Cv, 04.25.Gy, 11.10.-z

In Refs. [1, 2] the possibility in principle is shown that noncompensated Casimir force can exist in open nanosized metal cavities. The effect is theoretically demonstrated with a single trapezoid configuration. The force manifests itself as time-constant expulsion of open cavities in the direction of their least opening. Optimal parameters have been found for the angles of opening (broadening) of the cavities' generatrices and their lengths, at which the expulsion force is maximal. Note that this force significantly differs from repulsion forces capable of creating only the levitation-type effects over bodies-partners [3–7]. A particular case of such configurations is classical Casimir parallel mirrors [8–12]. It has been found that the ends of metal mirrors act as Casimir expulsion forces parallel to surfaces, which make 1/5 of the specific Casimir pressure [4]. However, these forces are completely compensated, i.e. in the entire configuration of parallel mirrors the effective force of expulsion does not exist in either direction. An interesting question arises whether it is possible that the balance of the forces of expulsion will change in trapezoid and parallel configurations when the planes shift relative to one another. The possibility of the evaluation of the influence of the planes' shift [13] upon the transverse Casimir force is also important.

## Theory

Let us consider a configuration with trapezoid cavities with shifted wings using it for investigating the possibility of the existence of Casimir expulsion forces. Note that each single cavity should be understood as an open thin-walled metal shell composed of metal flat plates (wings) with one or several outlets. Inner and outer surfaces of the cavity should have the properties of perfect mirrors. The cavity can completely be immersed into a material medium or be its part with the dielectric permeability properties differing from those of physical vacuum.

Let us present a single trapezoid configuration in Cartesian coordinates as two thin metal plates with the

surface width  $L$  (oriented along the  $z$  axis) and length  $R$  (a wing) situated at the distance  $a$  from one another; the angle  $\varphi$  of the cavities' opening between the plates can be changed (simultaneously for both wings of the trapezoid cavity by the same value) as it is shown in Fig.1. Let us also take into account the possibility of the shift of one of the cavity wings in the direction opposite to the  $x$  axis by step  $\Delta x$ . For the given problem geometry, the angle  $\varphi$  should not exceed the value  $\varphi \leq \text{arccot}(\Delta x/a)$ , otherwise the situation can occur when the configuration of cavities with two neighboring cavities is formed. This situation requires somewhat different problem statement. Note that further the concept developed in Ref. [1] is fully applicable for the above cavities. Thus, for one cavity wing, in the first approximation the expulsion force in the  $x$  direction can be found in the form [1]

$$F_x = \int_0^L dy \int_0^R P_x(\varphi, \Theta, r) dr. \quad (1)$$

Here the local specific force of expulsion at every point on the cavity wing with the length  $R$  and width  $L$  is

$$P_x = -\frac{\hbar c \pi^2}{240 s^4} \int_{\Theta_1}^{\Theta_2} \sin(\Theta - 2\varphi)^4 \cos(\Theta - \varphi) d\Theta \\ = -\frac{\hbar c \pi^2}{240 s^4} A_2(\varphi, \Theta_1, \Theta_2), \quad (2)$$

where

$$A_2(\varphi, \Theta_1, \Theta_2) \\ = \frac{1}{240} \left[ 90 \sin(\varphi - \Theta_1) - 90 \sin(\varphi - \Theta_2) \right. \\ + 60 \sin(3\varphi - \Theta_2) - 60 \sin(3\varphi - \Theta_1) \\ + 20 \sin(5\varphi - 3\Theta_2) - 20 \sin(5\varphi - 3\Theta_1) \\ + 5 \sin(7\varphi - 3\Theta_1) - 5 \sin(7\varphi - 3\Theta_2) \\ \left. + 3 \sin(9\varphi - 5\Theta_1) - 3 \sin(9\varphi - 5\Theta_2) \right]. \quad (3)$$

In formula (2)  $\hbar = h/2\pi$  is reduced Planck constant,  $c$  is light velocity; functional expressions for the limit angles  $\Theta_1, \Theta_2$  in the trapezoid cavity and the parameter  $s$  are

\* e.g.fateev@gmail.com

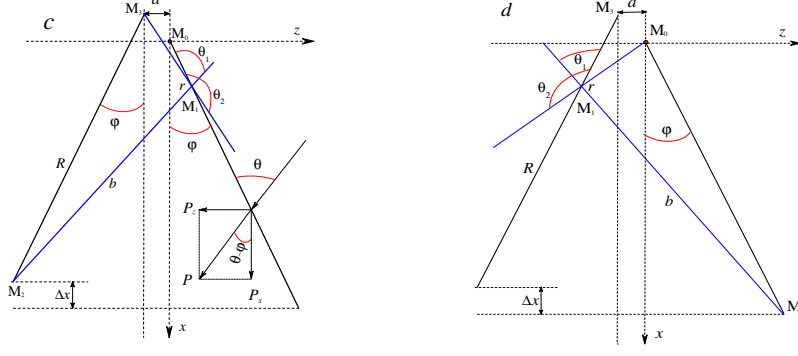


FIG. 1. *c* - schematic view of the configuration of the symmetric trapezoid cavity with the left wing (with the length  $R$ ) shifted by step  $\Delta x$  against the  $x$  axis, a particular case of which are parallel wings (for  $\varphi = 0$ ) and a triangle (at  $a = 0$  and  $\Delta x = 0$ ). The cavity with the width  $L$  in the  $y$  direction is shown in the Cartesian coordinates  $(x, z)$ . Blue straight lines designate virtual rays with length  $b$  going from a point  $M_1$  under the limit angle  $\Theta_1$  and  $\Theta_2$  to the right surface of the cavity and ending at the ends of the opposite cavity wing at points  $M_2$  and  $M_3$ , respectively; *d* - a scheme of the rays going under the limit angles  $\Theta_1$  and  $\Theta_2$  from a random point  $M_1$  on the left wing to the ends of the right wing.

as follows

$$\Theta_1 = \arccos \left( -\frac{r + a \sin \varphi - R \cos 2\varphi}{\sqrt{(a + R \sin \varphi + r \sin \varphi)^2 + (r \cos \varphi - R \cos \varphi)^2}} \right), \quad (4)$$

$$\Theta_2 = \arccos \left[ -\frac{r + a \sin \varphi}{\sqrt{a^2 + r^2 + 2r(a \sin \varphi)}} \right], \quad (5)$$

$$s = \frac{\sin(2\varphi - \Theta_2)(a + r \sin \varphi)}{\sin(\varphi - \Theta_2)}. \quad (6)$$

For the trapezoid figure the Casimir force in the  $z$  direction can be found in the form [1]

$$F_z = \int_0^L dy \int_0^R P_z(\varphi, \Theta, r) dr. \quad (7)$$

Here, at every point  $r$  on the cavity wing the specific Casimir force in the  $z$  direction is

$$\begin{aligned} P_z(r) &= -\frac{\hbar c \pi^2}{240 s^4} \int_{\Theta_1}^{\Theta_2} \sin(\Theta - 2\varphi)^4 \sin(\Theta - \varphi) d\Theta \\ &= -\frac{\hbar c \pi^2}{240 s^4} A_1(\varphi, \Theta_1, \Theta_2), \end{aligned} \quad (8)$$

where

$$\begin{aligned} A_1(\varphi, \Theta_1, \Theta_2) &= \frac{1}{240} \left[ 90 \cos(\varphi - \Theta_1) - 90 \cos(\varphi - \Theta_2) \right. \\ &+ 60 \cos(3\varphi - \Theta_2) - 60 \cos(3\varphi - \Theta_1) \\ &+ 20 \cos(5\varphi - 3\Theta_2) - 20 \cos(5\varphi - 3\Theta_1) \\ &+ 5 \cos(7\varphi - 3\Theta_1) - 5 \cos(7\varphi - 3\Theta_2) \\ &\left. + 3 \cos(9\varphi - 5\Theta_1) - 3 \cos(9\varphi - 5\Theta_2) \right]. \end{aligned} \quad (9)$$

To take into account the possibility of the influence of the left cavity wing shifts  $\Delta x$  relative to the right wing on the Casimir forces, it is necessary to find new functional expressions for the limit angles  $\Theta_1$ ,  $\Theta_2$ . Let us use the presentation of the directing vectors corresponding to the rays for the limit angles  $\Theta_1$ ,  $\Theta_2$  and the generatrix of the right cavity wing on the scheme of the trapezoid configuration (Fig.1c). Let us designate the point data on the plan of the trapezoid cavity:  $M_0(x_0, z_0)$ ,  $M_1(x_1, z_1)$ ,  $M_2(x_2, z_2)$  and  $M_3(x_3, z_3)$ . Then the vector  $\overrightarrow{M_0 M_1} = (x_1 - x_0; z_1 - z_0)$  can be chosen as a directing vector of the generatrix of the right cavity wing.  $\overrightarrow{M_1 M_2} = (x_2 - x_1; z_2 - z_1)$  is chosen as a directing vector of the straight line  $b$ .  $\overrightarrow{M_1 M_3} = (x_3 - x_1; z_3 - z_1)$  is chosen as a vector of the straight line between the extreme upper point of the left wing  $M_3(x_3, z_3)$  and the point  $M_1(x_1, z_1)$ . The corresponding coordinates can be written in the form:  $x_0 = 0$ ;  $z_0 = 0$ ;  $x_1 = r \cos \varphi$ ;  $z_1 = r \sin \varphi$ ;  $x_2 = R \cos \varphi - \Delta x$ ;  $z_2 = -R \sin \varphi - a$ ;  $x_3 = -\Delta x$ ;  $z_3 = -a$ . The cosines of the angles between the directrices are determined as follows

$$\begin{aligned} \cos \Theta_1^{right} &= \mp \frac{\overrightarrow{M_0 M_1} \cdot \overrightarrow{M_1 M_2}}{\|\overrightarrow{M_0 M_1}\| \cdot \|\overrightarrow{M_1 M_2}\|} \\ &= \pm \frac{(x_1 - x_0)(x_2 - x_1) + (z_1 - z_0)(z_2 - z_1)}{\sqrt{(x_1 - x_0)^2 + (z_1 - z_0)^2} \sqrt{(x_2 - x_1)^2 + (z_2 - z_1)^2}}, \end{aligned}$$

and

$$\begin{aligned} \cos \Theta_2^{right} &= \mp \frac{\overrightarrow{M_0 M_1} \cdot \overrightarrow{M_1 M_3}}{\|\overrightarrow{M_0 M_1}\| \cdot \|\overrightarrow{M_1 M_3}\|} \\ &= \pm \frac{(x_1 - x_0)(x_3 - x_1) + (z_1 - z_0)(z_3 - z_1)}{\sqrt{(x_1 - x_0)^2 + (z_1 - z_0)^2} \sqrt{(x_3 - x_1)^2 + (z_3 - z_1)^2}}. \end{aligned}$$

Now let us find the angles  $\Theta_1^{right}$  and  $\Theta_2^{right}$  in the form

$$\Theta_1^{right} = \arccos \left[ \frac{r+a \sin \varphi + \Delta x \cos \varphi - R \cos 2\varphi}{-\sqrt{[a+(R+r) \sin \varphi]^2 + [\Delta x + (r-R) \cos \varphi]^2}} \right], \quad (10)$$

$$\Theta_2^{right} = \arccos \left[ \frac{r+a \sin \varphi + \Delta x \cos \varphi}{-\sqrt{a^2 + \Delta x^2 + r^2 + 2a r \sin \varphi + 2\Delta x r \cos \varphi}} \right]. \quad (11)$$

To obtain the integral dependencies of expulsion and

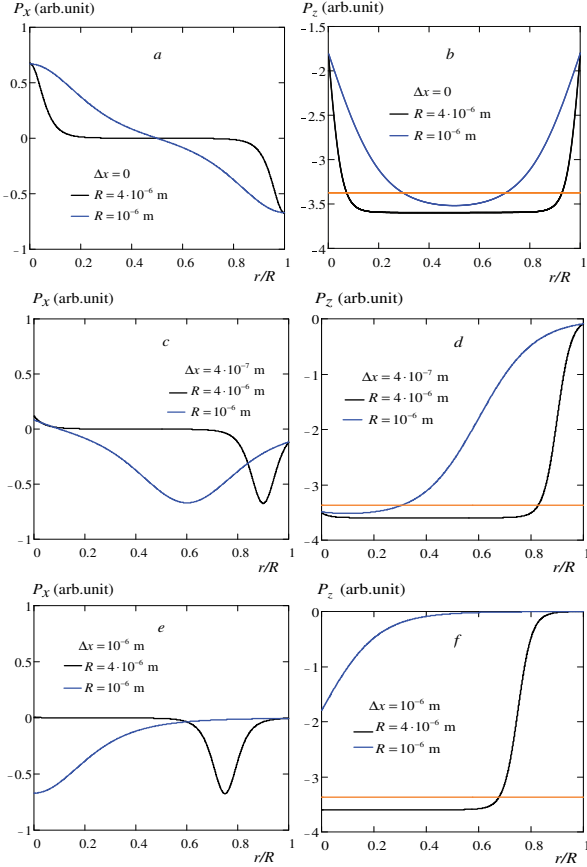


FIG. 2. Specific local forces of expulsion (a) and pressure (b) along the  $x$  axis for strictly parallel wings ( $\varphi = 0$ ) in the absence of shift. Respectively, local forces (c) and (d) at the shift of the cavity left wing for  $\varphi = 0$  by  $\Delta x = 4 \times 10^{-7}$  m. Local specific forces (e) and (f) at the shift of the cavity left wing by  $\Delta x = 10^{-6}$  m. The red line (b, d, f) shows the classical level of the Casimir pressure for  $a = 4 \times 10^{-7}$  m.

pressure for both wings of the cavity it is also necessary to find the corresponding limit angles for the rays going from the arbitrary points of the left wing to the ends of the right wing in the process of shift. It is clear that at the shift relative to the right wing, the point data  $M_0(x_0, z_0)$ ,  $M_1(x_1, z_1)$ ,  $M_2(x_2, z_2)$  and  $M_3(x_3, z_3)$  corresponding to the vectors  $\overrightarrow{M_0 M_1} = (x_1 - x_0; z_1 - z_0)$ ,  $\overrightarrow{M_1 M_2} = (x_2 -$

$x_1; z_2 - z_1)$ , and  $\overrightarrow{M_1 M_3} = (x_3 - x_1; z_3 - z_1)$  going from the left wing of the cavity (see Fig.1d) will differ from those for the right wing. Let us write them down:  $x_0 = 0; z_0 = 0; x_1 = r \cos \varphi - \Delta x; z_1 = -r \sin \varphi - a; x_2 = R \cos \varphi; z_2 = R \sin \varphi; x_3 = -\Delta x; z_3 = -a$ . The corresponding cosines of the angles between the directrices of these vectors have the form

$$\begin{aligned} \cos \Theta_1^{left} &= \mp \frac{\overrightarrow{M_1 M_3} \cdot \overrightarrow{M_1 M_2}}{\|\overrightarrow{M_1 M_3}\| \cdot \|\overrightarrow{M_1 M_2}\|} \\ &= \pm \frac{(x_3 - x_1)(x_2 - x_1) + (z_3 - z_1)(z_2 - z_1)}{\sqrt{(x_3 - x_1)^2 + (z_3 - z_1)^2} \sqrt{(x_2 - x_1)^2 + (z_2 - z_1)^2}}, \end{aligned}$$

and

$$\begin{aligned} \cos \Theta_2^{left} &= \mp \frac{\overrightarrow{M_0 M_3} \cdot \overrightarrow{M_0 M_1}}{\|\overrightarrow{M_0 M_3}\| \cdot \|\overrightarrow{M_0 M_1}\|} \\ &= \pm \frac{(x_1 - x_0)(x_3 - x_1) + (z_1 - z_0)(z_3 - z_1)}{\sqrt{(x_1 - x_0)^2 + (z_1 - z_0)^2} \sqrt{(x_3 - x_1)^2 + (z_3 - z_1)^2}}. \end{aligned}$$

Let us find the angles  $\Theta_1^{left}$  and  $\Theta_2^{left}$  in the form

$$\Theta_1^{left} = \pi - \arccos \left[ \frac{R+r+a \sin \varphi - \Delta x \cos \varphi - 2R \cos^2 \varphi}{-\sqrt{[a+(R+r) \sin \varphi]^2 + [\Delta x + (r-R) \cos \varphi]^2}} \right], \quad (12)$$

$$\Theta_2^{left} = \arccos \left[ \frac{r+a \sin \varphi - \Delta x \cos \varphi}{-\sqrt{a^2 + \Delta x^2 + r^2 + 2a r \sin \varphi - 2\Delta x r \cos \varphi}} \right]. \quad (13)$$

In this case the change of the parameter  $s$  will correspond to formula (5). Thus, the forces acting upon the entire configuration at the shift of the wings relative to one another (if the configuration is fixed in a new position after the shift) are the sum of the corresponding forces for the right and left wings of the cavity

$$F_x = F_x^{right} + F_x^{left} \quad \text{and} \quad F_z = F_z^{right} + F_z^{left}. \quad (14)$$

### Calculation results

Using formulae (1-14) it is possible to find the character of the specific Casimir forces  $P_z(r)$  and  $P_x(r)$  along the  $x$  axis for two parallel plates ( $\varphi = 0$ ) having the same length  $R$  and the distance  $a = 4 \times 10^{-7}$  m between them (see Fig.2). In Fig. 2 it can be seen that at  $R/a \geq 1$  on the figure boundaries the specific force  $P_z(r)$  is always less by half than that in the centre of the configuration (Fig. 2b). The smaller is the wing length  $R$ , the more inhomogeneous are the forces of compression. In addition it can be seen that there are forces  $P_x(r)$  in the configuration compressing the ends of the parallel plates toward their centers (Fig.2a).

The specific force of compression of the two parallel plates ( $\varphi = 0$ ) along the  $x$  axis makes up 3/8 of the Casimir pressure on the plates along the  $z$  axis. The smaller is the length  $R$ , the larger part of the cavity wing is subjected to the action of such forces. However, along the  $x$  axis the integral Casimir forces  $P_x(r)$  compensate one another, i.e. is the directed force does not act upon the entire configuration in any direction. There will be

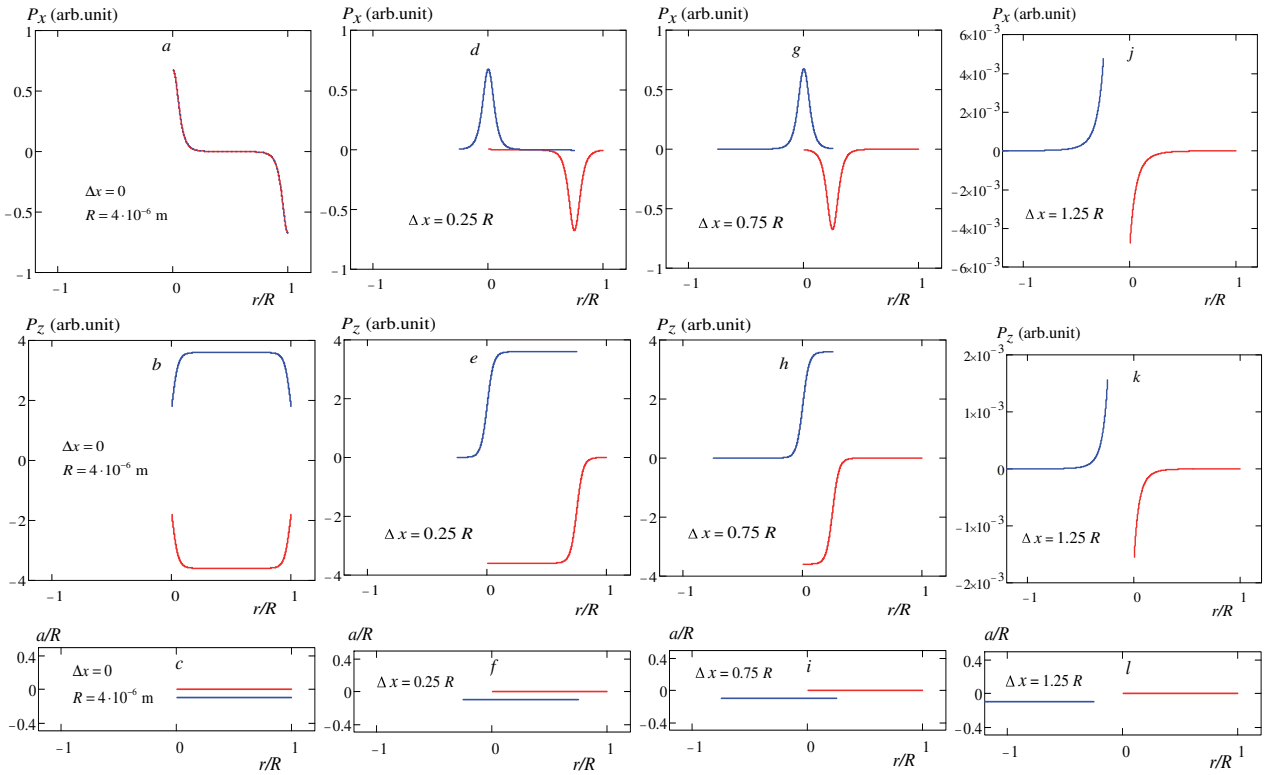


FIG. 3. Specific local forces of expulsion (*a*, *d*, *g*, *j*) and pressure (*b*, *e*, *h*, *k*) along the  $x$  axis for strictly parallel plates ( $\varphi = 0$ ) at different relative shifts  $\Delta x/R$ . In the figure, the red lines show the dependences of the local forces corresponding to the right plates (red) (*c*, *f*, *i*, *l*), and the blue lines show the dependences corresponding to the left plates (blue).

similar character of dependences at the rescaling of dimensional parameters of the configuration to any small values within physically reasonable limits restricted by sizes of atoms.

In Fig.2c it is seen that at the shift of the left plate by the quantity  $\Delta x = 4 \times 10^{-7}$  m against the  $x$  axis, forces of expulsion become uncompensated on the right plate. In this case, the local expulsive forces of the right plate in the  $x$  direction decrease starting from the point  $r = 0$ ; however, at the point  $(R - \Delta x)/R$  an extremum appears. From Fig.2d it also follows that for  $r = 0$  at the end of the right plate at the shift  $\Delta x = 4 \times 10^{-7}$  m the Casimir pressure grows practically to the values characteristic of points close to  $r = R/2$ .

Obviously, noncompensated Casimir force in the  $x$  direction will appear on the left plate, which is similar to that found on the right plate (see Fig. 3), which is however oppositely directed. It means that at the shift of the left plate by  $\Delta x$  against the  $x$  axis, forces appear in the configuration, which tend to bring the plate back to the state before the shift to the value  $\Delta x = 0$ . In addition, the same forces will create a clockwise torque around the center of mass of the configuration in the plane  $(x, z)$  parallel to the  $y$  axis. In contrast to the expulsive forces, the Casimir pressure along the  $z$  axis will have a symmetric form relative to the configuration centre at any shift of

the plates (Fig.3b, *e*, *h*, *k*). Let us suppose that after shift the plates will be fixed; in this case in the system the clockwise torque will appear in the plane  $(x, z)$  due to the Casimir forces of expulsion. However, if the system is not fixed along the  $x$  axis after shift and let us suppose that the distance  $a$  remains constant, the appearance of rather complex oscillatory motions can be expected in the system. The oscillations of such system can have the following character. After the shift by  $\Delta x$ , both plates will tend to return to the previous state when  $\Delta x = 0$  and simultaneously will spin together in the clockwise direction in the plane  $(x, z)$ . Obviously, the plates will return to the opposite state with the shift  $-\Delta x$  along the  $x$  axis. When imperfect systems are considered, it is necessary to take into account the processes of dissipation in them. In this case the system will return to the state which is not absolutely opposite with the shift by  $-\Delta x$  relative to the  $x$  axis. Thus, the system of the plates will tend in the direction opposite to the shift motion and simultaneously it will spin in the opposite (anticlockwise) direction. That is in the unfixed system of plates, after the shift of the plates relative to one another complex cyclic processes can be observed.

When the cavity wings are open up to the permissible limit angle  $\varphi \leq \text{arccot}(\Delta x/a)$ , with growing  $r/R \rightarrow 1$  the specific forces are decreasing both along the  $x$  axis

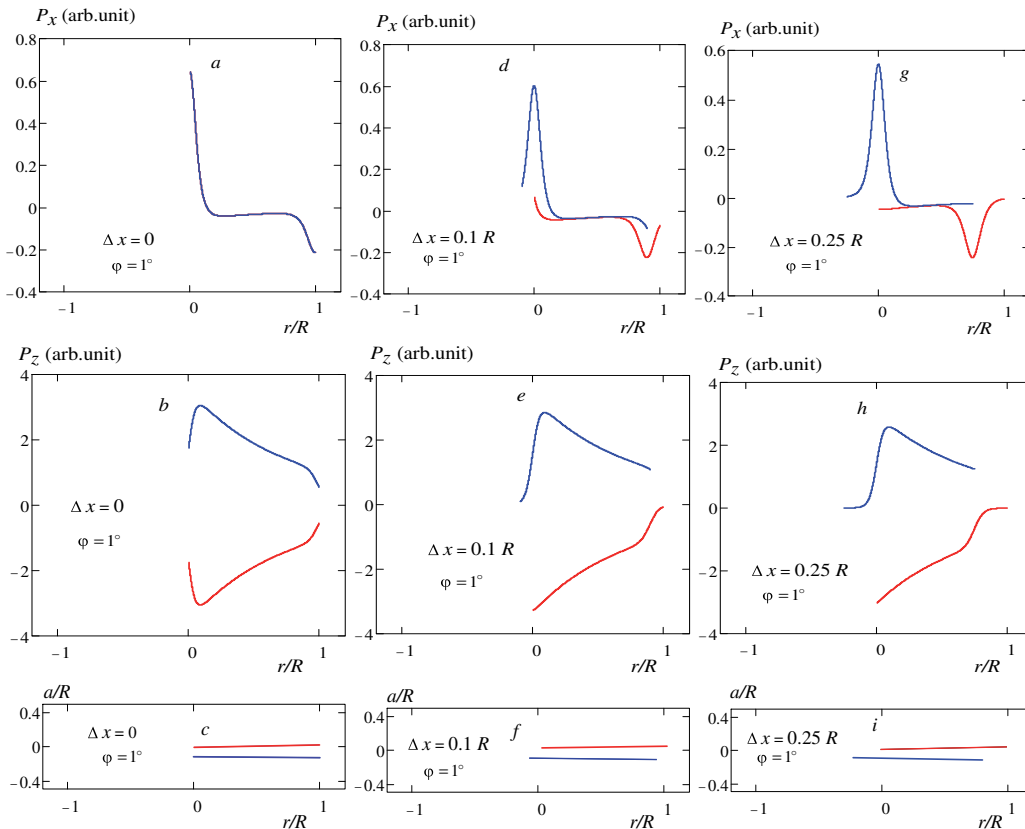


FIG. 4. Specific local forces of expulsion ( $a, d, g$ ) and pressure ( $b, e, h$ ) along the  $x$  axis for the plates ( $\varphi = 1^\circ$ ) at different relative shifts  $\Delta x/R$ . In the figure, red lines show the dependences of the local forces corresponding to the left plates ( $c, f, i$ ) and the blue lines show the dependences corresponding to the right plates.

and along the  $z$  axis (Fig.4a, b). However, the character of the spinning action of the forces on the plates weakens with the growth of the angle  $\varphi$  and the direction of the shifting forces remains similar to that which is observed in the case of parallel plates. Such character of the weakening of the forces at the shift of planes and the simultaneous increase of the angle of their opening  $\varphi$  significantly differs from that observed in the situation when there is no shift (see Fig.3).

By integrating  $P_x(r)$  and  $P_z(r)$  with respect to  $x$  we find the total Casimir force  $F_x$  and  $F_z$  acting on the right wing of the cavity at the shift of the left wing. Let us investigate the dependence of the Casimir forces on the wing length  $R$ . Also, let us find the most effective wing length at which there is the maximum of the function and the relation  $F_x/F_z$ . The corresponding results are displayed in Fig.5.

As seen in Fig. 5a, the total expulsive force of the shifted configuration is always directed against the  $x$  axis similar to the case of the configuration without shift. The force manifests itself as time-constant expulsion of opened trapezoid cavity in the direction of its least opening (i.e. in the direction of the smaller section). The forces grow with the growth of the cavity wing length to a

certain best length  $R_{eff}$  (Fig.5c), after which the growth of the forces continue but the relation of the forces to the wing length decreases. It means that the expulsion force is most effectively manifested in the region limited by the size  $R_{eff}$ . For the configurations without shifts, at the angle  $\varphi = 1^\circ$  this optimum has the theoretical value  $R_{eff} = 1.85 \times 10^{-9}$  m (1.85 nm) and, correspondingly,  $F_x \sim 5.7$  N for one cavity wing with  $R = R_{eff}$  and the length  $l = 1$  m. However, at a small shift of the left plate ( $\Delta x/a = 0.5$ ) the entire force of the figure expulsion grows to the values  $F_x \sim 21$  N. Such shift in the configuration leads to a considerable decrease in the theoretical value  $R_{eff}$  down to  $R_{eff} \sim a$  (0.4 nm). Here the values of forces are given in real quantities.

Note that the shift does not influence the character of the growth of the Casimir pressure at the growth of the cavity wing length  $R$ . The relation of total expulsive forces to the compressive forces  $F_x/F_z$  acquires radically different character depending on the wing length  $R$  at the shift in the configuration (Fig. 5d). Instead of gradual growth of the value  $|F_x/F_z|$  up to  $|F_x/F_z| \rightarrow 4.2 \times 10^{-3}$ , at the shift of the plates by  $\Delta x/a = 0.5$  the theoretical relation  $|F_x/F_z|$  decreases from the value  $|F_x/F_z| \sim 10^2$  to  $|F_x/F_z| \rightarrow 1.3 \times 10^{-2}$ . For the value  $R_{eff} \sim a$  the

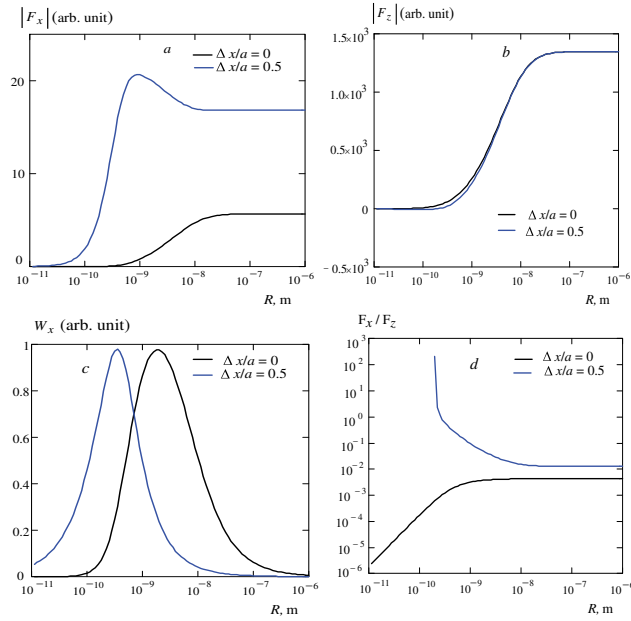


FIG. 5. The total Casimir force of expulsion (*a*) and compression (*b*) of the cavity wing at  $\varphi = 1^\circ$  depending on the wing length  $R$  and at the  $\Delta x/R$  shift of the left plate relative to the right one. The dependence of the effectiveness of the expulsion  $W_x$  on the wing length (*c*) at the shift. The relation of the total forces of expulsion to the forces of compression  $F_x/F_z$  depending on the wing length  $R$  (*d*).

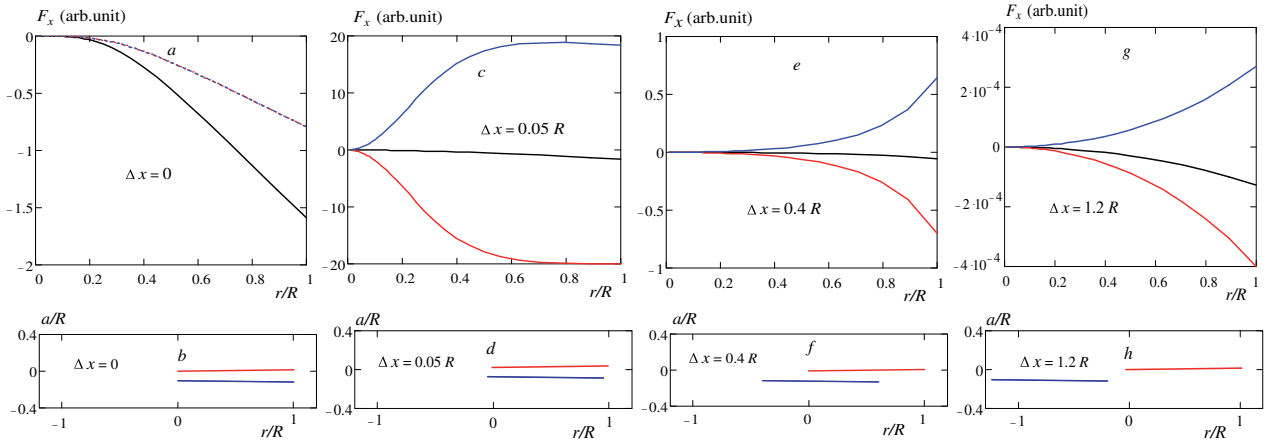


FIG. 6. The Casimir force of expulsion of the entire configuration of the cavity wings (*a*, *c*, *e*, *g*) fixed after the shift for  $\varphi = 1^\circ$  depending on the length  $r$  of the wings and the shift  $\Delta x/R$  of the left plate (*b*, *d*, *f*, *h*) (red line) relative to the right plate (blue line). The black line shows the integral force of expulsion of the configuration fixed after the shift.

relation is  $|F_x/F_z| \approx 0.46$ .

The Casimir forces of expulsion for the entire configuration (if after the shift of the wings the configuration is fixed in the new position) with the angle of opening  $\varphi = 1^\circ$  at different  $\Delta x$  are shown in Fig.6 depending on the length of the wings. In the absence of shift ( $\Delta x = 0$ ) both wings expelled against the  $x$  direction (Fig. 6*a*, *b*). If the wings are rigidly connected the configuration is expelled against the  $x$  axis in two times stronger. Even a very small shift of the left plate relative to the right

plate (for example, by  $\Delta x/R = 0.05$ ) leads to an abrupt change in the direction and value of the expulsive forces. The left wing is expelled in the  $x$  direction and the right wing against the  $x$  axis with the force larger by a factor of 10 than that in the absence of shift (Fig.6*c*, *d*). In this case the integral force of the expulsion of the fixed configuration is directed against the  $x$  axis, and its value makes  $\sim 99\%$  of that of the force before the shift. At the shift of the order of  $\Delta x/R = 0.4$  the system of two connected plates is also expelled against the  $x$  axis but

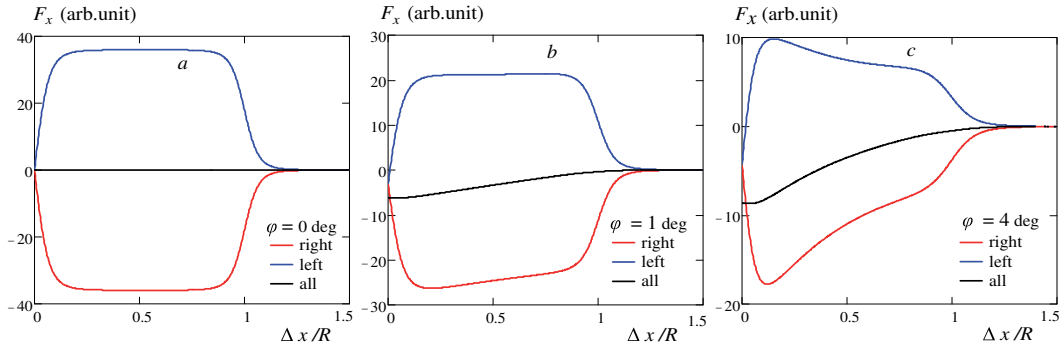


FIG. 7. The dependences of the forces of expulsion of the right  $F_x^{right}$  wing and the left  $F_x^{left}$  wing and the sum of these forces  $F_x$  on the value of the shift  $\Delta x/R$  for three angles of the opening of the generatrices of the wings.

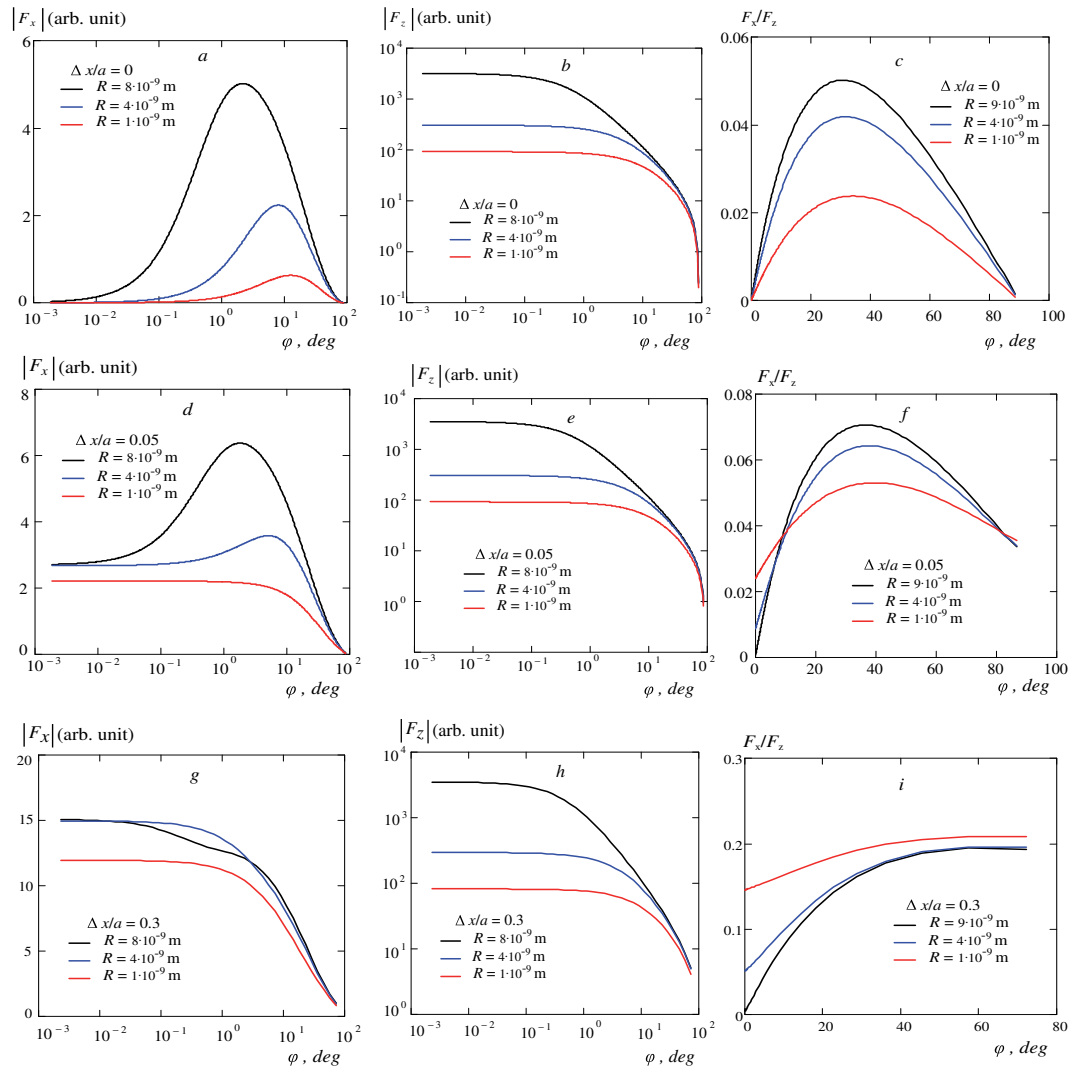


FIG. 8. Absolute values of the Casimir forces of expulsion (a) and compression (b) for different lengths  $R$  depending on the angle  $\varphi$  for the configurations without shift  $\Delta x/a = 0$ . (c) – the relation of the total forces of expulsion to the compression depending on the angle  $\varphi$ . The corresponding forces and relations for the configuration with the shift  $\Delta x/a = 0.05$  (d, e, f) and  $\Delta x/a = 0.3$  (g, h, i).

much weaker (Fig.6e, f) than in the case of smaller shifts.

At  $\Delta x/R = 1.2$  and larger shifts (by  $\Delta x/R \gg 1$ ) the integral forces of expulsion retain the direction but rapidly become weaker to 0. At the increase of the angle  $\varphi$  the direction of the expulsive forces remains the same but the integral forces become even weaker. This also follows from the shift value  $\Delta x/R$  dependence of the forces of expulsion of the right  $F_x^{right}$  and left  $F_x^{left}$  wings and the sum of these forces  $F_x = F_x^{right} + F_x^{left}$  in the configuration fixed after the shift (Fig.7).

Figure 8a, b shows the dependences of the integral forces of expulsion and compression of the configuration right wing on the angle  $\varphi$ . It can be seen that in the absence of shift for any length  $R$  of the cavity wing  $\Delta x/a = 0$  there is the maximum of compulsion depending on the angle  $\varphi$ . The larger is the length  $R$ , the smaller is the angle. Fig. 8c presents the relation  $F_x/F_z$  depending on the angle  $\varphi$ .

Even though the shift of the configuration is  $\Delta x/a = 0.05$ , a significant change in the character of the angle  $\varphi$  dependences of the forces of expulsion takes place (Fig. 8d). However, the character of the Casimir along the  $x$  axis does not practically change at the configuration shift (Fig.8e, h). When the shift by  $\Delta x/a = 0.3$  takes place, a considerable growth of expulsive forces is observed for very small angles  $\varphi$  of the opening of cavities. Most clearly it can be observed for the lengths  $R_{eff} \leq a$  (Fig.8g).

## Conclusions

In the present paper, it is shown that the shifts in configurations of trapezoid metal (perfectly conducting) nanosized cavities lead to significant changes in the character of dependences of the noncompensated Casimir forces (forces of expulsion) on the length of wings and the angles of their opening. At such shifts the character of the change in the Casimir pressure does not practically depend on the wings' length and the angles of their opening. In the case of parallel metal mirrors, it is found that after the shift in both plates the appeared forces of expulsion are directed so that they are tending to return the system in the state before the shift. In the case of the unfixed arrangement of plates relative one another at the fixed distance, after shifts complex oscillatory states with torques can appear in the system of the plates. In the case of the arrangement of plates the direction of expulsion can change in configurations depending on the degree of the shift of their elements. At any shift of elements a time-constant torque can appear in a configuration.

## ACKNOWLEDGMENTS

The author is grateful to T. Bakitskaya for hers helpful participation in discussions.

- 
- [1] E.G. Fateev, arXiv:1208.0303v1(2012).
  - [2] E.G. Fateev, arXiv:1208.1256v1(2012).
  - [3] R. L. Jaffe, A. Scardicchio, J. High Energy Phys. V.06 (2005).
  - [4] U. Leonhardt, New J. Phys. **9**, 254 (2007).
  - [5] M. Levin, A. P. McCauley, A. W. Rodriguez, M. T. Homer Reid, and S. G. Johnson, Phys. Rev. Lett. **105**, 090403 (2010). (4 pages).
  - [6] S. J. Rahi, T. Emig, R. L. Jaffe, arXiv:1007.4355v1 (2010).
  - [7] S. J. Rahi, S. Zaheer, Phys. Rev. Lett. **104**, 070405 (2010).
  - [8] H. B. G. Casimir, Kon. Ned. Akad. Wetensch. Proc. **51**, 793 (1948).
  - [9] H. B. G. Casimir and D. Polder, Phys. Rev. **73**, 360 (1948).
  - [10] K. A. Milton, *The Casimir effect: Physical manifestations of zero-point energy*, World Scientific, Singapore, 2001.
  - [11] G. L. Klimchitskaya, U. Mohideen, and V. M. Mostepanenko, Rev. Mod. Phys. **81**, 1827 (2009).
  - [12] M. Bordag, G. L. Klimchitskaya, U. Mohideen, and V. M. Mostepanenko, *Advances in the Casimir effect*, Oxford University Press, Oxford, 2009.
  - [13] H. Gies, K. Klingmuller, Phys. Rev. Lett. **97**, 220405 (2006).